3.3. Powder diffraction peak profiles

R. B. Von Dreele

3.3.1. Introduction

The analysis of a powder diffraction pattern usually involves the fitting of a model to the set of peaks that are found in that pattern. The desired result may be accurate peak positions to be used as input for an indexing procedure, or extraction of the suite of reflection intensities for crystal structure determination or a Rietveld refinement. In any case, a good description of the shape of the powder peak profile and how it varies across the entire pattern is of paramount importance for obtaining the highest-quality results, and this topic was briefly reviewed in Volume C of *International Tables for Crystallography* (Parrish, 1992).

The fitting is a least-squares procedure in which the model used to calculate the intensity of the profile is

$$Y(x) = \sum_j I_j P_j(\Delta) + B(x), \tag{3.3.1}$$

where I_j is the integrated intensity of the jth peak and P is the shape function for that peak, which depends on the offset ($\Delta = x - T_j$) of its position T_j from the observation point x. The sum is over all reflections that could contribute to the profile and $B(x)$ is a background intensity function. The observed shape of the peaks arises from a convolution of the intrinsic source profile (G_λ), the various instrumental profile contributions (G_I) (*e.g.* from slits and monochromators, discussed in Chapter 3.1) and the characteristics of the sample (G_S) that broaden the idealized reciprocal-space points (see Chapter 3.6):

$$P(\Delta) = G_\lambda * G_I * G_S. \tag{3.3.2}$$

In practice, the peak profile function is usually developed by either selecting a peak-shape function that has the required shape characteristics to fit the experimental peak profiles (the semi-empirical function approach, or SFA) or by selecting a number of contributing functions and doing the requisite convolutions (the fundamental parameters approach, or FPA) (Cheary & Coelho, 1998*b*).

Both approaches have been used for the analysis of constant-wavelength neutron and X-ray powder diffraction data and for neutron time-of-flight (energy-dispersive) powder data. In addition, the peaks can be seen to be displaced from their expected positions given by Bragg's law. As we will see, this displacement is partially a consequence of some geometric features of the experiment but is also dependent upon the particular description of the peak profile.

3.3.2. Peak profiles for constant-wavelength radiation (X-rays and neutrons)

3.3.2.1. *Introduction – symmetric peak profiles*

The realization that the neutron powder diffractometer at the Reactor Centrum Nederland, Petten, produced powder peak profiles that were Gaussian in shape led Rietveld (1967) to develop a full-pattern method for crystal structure refinement (Rietveld, 1967, 1969), now known as the Rietveld refinement method. The Gaussian is formulated as

$$P_G(\Delta, \Gamma_G \text{ or } \sigma^2) = \frac{(8\ln 2)^{1/2}}{\Gamma_G(2\pi)^{1/2}} \exp\left(\frac{-4\ln 2\Delta^2}{\Gamma_G^2}\right) = \frac{1}{(2\pi\sigma^2)^{1/2}} \exp\left(\frac{-\Delta^2}{2\sigma^2}\right), \tag{3.3.3}$$

where the width of the peak is expressed as either the full width at half-maximum (FWHM = Γ_G) or as the variance (σ^2). Rietveld also recognized the earlier analysis of the resolution of a neutron powder diffractometer by Caglioti *et al.* (1958), who showed that the contributions from the source size, collimators and monochromator crystal mosaic spread and scattering angle could be combined analytically to give

$$\Gamma_G^2 = U\tan^2\theta + V\tan\theta + W \tag{3.3.4}$$

with U, V and W adjustable during the Rietveld refinement. A modified form of this may have more stability in refinement (attributed to E. Prince by Young & Wiles, 1982):

$$\Gamma_G^2 = U'(\tan\theta - K_0)^2 + V'(\tan\theta - K_0) + W', \tag{3.3.5}$$

where K_0 is arbitrarily chosen as 0.6.

Improvements in the resolution of neutron powder diffractometers and (more importantly) attempts to apply the Rietveld method to X-ray powder diffraction data required the development of new powder profile functions (Malmros & Thomas, 1977; Young *et al.*, 1977; Young & Wiles, 1982); this is because the Gaussian function [equation (3.3.3)] gave poor fits to observed peak profiles, partially because of the Lorentzian emission line profile (G_λ) from laboratory X-ray tubes. Many functions were considered, including Lorentzian ('Cauchy'), various modified Lorentzians, Pearson VII and pseudo-Voigt. Of these the last two performed (on individual peak fits) about equally well; functional forms are:

Lorentzian 'Cauchy' function

$$P_L(\Delta, \Gamma_L) = \left(\frac{\Gamma_L}{2\pi}\right)\left\{\frac{4}{\left[\Gamma_L^2 + (2\Delta)^2\right]}\right\}, \tag{3.3.6}$$

Pearson VII function

$$P_{\rm P7}(\Delta, \xi, \mu) = \frac{\Gamma(\mu)}{\xi\Gamma\left(\mu - \frac{1}{2}\right)(\mu\pi)^{1/2}} \Big/ \left(1 + \frac{\Delta^2}{\mu\xi^2}\right)^{\mu}, \tag{3.3.7}$$

pseudo-Voigt function

$$P_{\rm PV}(\Delta, \Gamma, \eta) = \eta P_L(\Delta, \Gamma) + (1 - \eta)P_G(\Delta, \Gamma), \tag{3.3.8}$$

where Γ_L is the FWHM of the Lorentzian peak and $\Gamma(\mu)$ in the Pearson VII function is the Gamma function; μ may vary between 0 and ∞, and μ is the half width at $(1 + 1/\mu)^{-\mu}$ of the peak height (David, 1986); $P_{\rm P7}(\Delta, \Gamma, 1) \simeq P_L(\Delta, \Gamma)$ and $P_{\rm P7}(\Delta, \Gamma, \infty) \simeq P_G(\Delta, \Gamma)$. Although the Pearson VII function performs well in individual peak fits, it is of little use for Rietveld refinements because of the difficulty in relating its coefficients to physically meaningful characteristics of the sample and will not be considered further in this discussion.

The pseudo-Voigt function is an approximation to the Voigt function, which is the convolution of a Gaussian and a Lorentzian:

Voigt function

$$P_V(\Delta, \Gamma_L, \Gamma_G) = \int_{-\infty}^{\infty} P_L(\Delta, \Gamma_l) P_G(\Delta - \delta, \Gamma_G)\, \mathrm{d}\delta$$
$$= \left(\frac{4 \ln 2}{\pi \Gamma_G^2}\right)^{1/2} \mathrm{Re}[\exp(-z^2)\mathrm{erfc}(-iz)], \quad (3.3.9)$$

where $z = \alpha + i\beta$, $\alpha = (4 \ln 2)^{1/2} \Delta/\Gamma_G$ and $\beta = (\ln 2)^{1/2} \Gamma_L/\Gamma_G$.

A number of formulations have been proposed for the pseudo-Voigt coefficients to make the best fit to the corresponding Voigt function (Hastings *et al.*, 1984; David, 1986; Thompson *et al.*, 1987). The latter is most commonly used and gives overall the FWHM, Γ and the mixing coefficient, η, to be used in equation (3.3.8) as functions of the individual FWHMs Γ_G and Γ_L:

$$\Gamma = [(\Gamma_G^5 + 2.69269\Gamma_G^4\Gamma_L + 2.42843\Gamma_G^3\Gamma_L^2 + 4.47163\Gamma_G^2\Gamma_L^3 + 0.07842\Gamma_G\Gamma_L^4 + \Gamma_L^5)]^{1/5}, \quad (3.3.10)$$

$$\eta = 1.36603(\Gamma_L/\Gamma) - 0.47719(\Gamma_L/\Gamma)^2 + 0.11116(\Gamma_L/\Gamma)^3. \quad (3.3.11)$$

The alternative given by David (1986) uses a more generalized version of the pseudo-Voigt function,

$$P_{\mathrm{PV}}(\Delta, W_G, W_L, \eta_G, \eta_L) = \eta_L P_L(\Delta, W_L) + \eta_G P_G(\Delta, W_G),$$
$$\eta_G = 0.00268\rho_1 + 0.75458\rho_1^2 + 2.88898\rho_1^3 - 3.85144\rho_1^4 - 0.55765\rho_1^5 + 3.03824\rho_1^6 - 1.27539\rho_1^7,$$
$$\eta_L = 1.35248\rho_2 + 0.41168\rho_2^2 - 2.18731\rho_2^3 + 6.42452\rho_2^4 - 10.29036\rho_2^5 + 6.88093\rho_2^6 - 1.59194\rho_2^7,$$
$$W_G = \Gamma(1 - 0.50734\rho_2 - 0.22744\rho_2^2 + 1.63804\rho_2^3 - 2.28532\rho_2^4 + 1.31943\rho_2^5),$$
$$W_L = \Gamma(1 - 0.99725\rho_1 + 1.14594\rho_1^2 + 2.56150\rho_1^3 - 6.52088\rho_1^4 + 5.82647\rho_1^5 - 1.91086\rho_1^6), \quad (3.3.12)$$

where $\Gamma = \Gamma_G + \Gamma_L$, $\rho_1 = \Gamma_G/\Gamma$ and $\rho_2 = \Gamma_L/\Gamma$; this is claimed to match the Voigt function to better than 0.3%.

3.3.2.2. *Constant-wavelength powder profile asymmetry*

Rietveld (1969) noted that at very low scattering angles the peaks displayed some asymmetry, which shifted the peak maximum to lower angles. He ascribed the effect to 'vertical divergence' and proposed a purely empirical correction for it. Subsequent authors (Cooper & Sayer, 1975; Howard, 1982; Hastings *et al.*, 1984) offered semi-empirical treatments of the profile shape that results from the intersection of a Debye–Scherrer cone with a finite receiving slit, which is described as 'axial divergence'. A more complete analysis of the problem in neutron powder diffraction was offered by van Laar & Yelon (1984), who considered the effect of a finite vertical slit ($2H$) intercepting a set of Bragg diffraction cones generated from a finite sample length ($2S$) within the incident beam for a goniometer radius (L). As seen in Fig. 3.3.1, this gives peak intensity beginning at $2\varphi_{\min} < 2\theta$ *via* scattering from only the ends of the sample; at $2\varphi_{\mathrm{infl}}$ the entire sample scatters into the detector. The resulting intensity profile is then convoluted with a Gaussian function to give the resulting asymmetric powder line profile (Fig. 3.3.2). This approach was then considered by Finger *et al.* (1994) for synchrotron powder diffraction and they created a Fortran code that was subsequently adopted *via* convolution with a pseudo-Voigt function [equation (3.3.12)] for use by many Rietveld refinement codes. Although originally formulated for parallel-beam neutron optics, it was shown by Finger *et al.* (1994) that it could be equally well applied to diverging X-ray and neutron optics by allowing the sample length to vary during the Rietveld refinement. They also showed that it could be applied to the asymmetry observed at low angles with Bragg–Brentano instrumentation. In that case the detector height is defined by the diffracted-beam Soller slits.

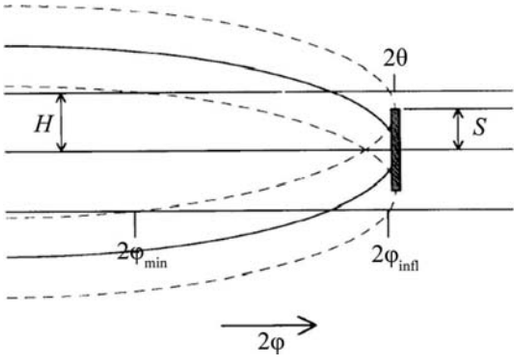

Figure 3.3.1
The band of intensity diffracted by a sample with height $2S$, as seen by a detector with opening $2H$ and a detector angle 2φ moving in the detector cylinder. For angles below $2\varphi_{\min}$ no intensity is seen. For angles between $2\varphi_{\mathrm{infl}}$ and 2θ, scattering from the entire sample can be seen by the detector. Figure and caption adapted from Finger *et al.* (1994).

Clearly, this asymmetric peak-shape function properly represents the offset of the peak top from the peak position, in contrast to functions such as the split Pearson VII function. Consequently, single peak fits using this function will give peak positions that are more readily indexed using methods such as those described in Chapter 3.4.

3.3.2.3. *Peak-displacement effects*

The position of the peak is also affected by various instrumental and geometric effects. For example, the sample position in a Bragg–Brentano experiment is ideally tangent to the focusing circle (Parrish, 1992). A radial displacement, s, of the sample will shift the Bragg peaks according to

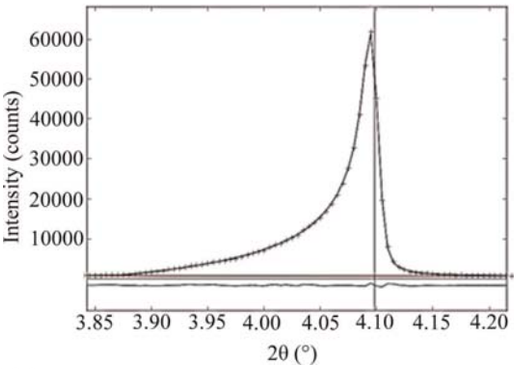

Figure 3.3.2
Low-angle synchrotron powder diffraction line ($2\theta \simeq 4.1^\circ$) fitted by the Finger *et al.* (1994) axial divergence powder line-shape function. The observed points (+), calculated curve, background and difference curves are shown. Note the offset of the peak top from the Bragg 2θ position (vertical line).

references